

Electron Magnetic Moment in Highly Charged Ions: The ARTEMIS Experiment

Manuel Vogel,* Mohammad Sadegh Ebrahimi, Zhexi Guo, Anahita Khodaparast, Gerhard Birkel, and Wolfgang Quint

The magnetic moment (*g*-factor) of the electron is a fundamental quantity in physics that can be measured with high accuracy by spectroscopy in Penning traps. Its value has been predicted by theory, both for the case of the free (unbound) electron and for the electron bound in a highly charged ion. Precision measurements of the electron magnetic moment yield a stringent test of these predictions and can in turn be used for a determination of fundamental constants such as the fine structure constant or the atomic mass of the electron. For the bound-electron magnetic-moment measurement, two complementary approaches exist, one via the so-called “continuous Stern–Gerlach effect”, applied to ions with zero-spin nuclei, and one a spectroscopic approach, applied to ions with nonzero nuclear spin. Here, the latter approach is detailed, and an overview of the experiment and its status is given.

1. Introduction

The magnetic moment $\vec{\mu}$ of an elementary particle is a fundamental intrinsic property. Precise measurements of magnetic moments of particles and their antiparticles yield stringent tests of matter–antimatter symmetries in nature. Such comparisons have, for example, been performed with the electron/positron and the proton/antiproton.^[1] Comparisons of precise measurements with similarly precise predictions by theory allow one to benchmark the underlying calculations and models, or in turn to extract fundamental quantities. For the electron bound in a highly charged ion, this concerns the fine structure constant, the atomic mass of the electron, and properties of the ion’s nucleus.^[1,2]

We express the magnetic moment $\vec{\mu}$ by the “*g*-factor” which is the dimensionless proportionality constant *g* between a

particle’s total angular momentum \vec{J} and its corresponding magnetic moment $\vec{\mu}$ as given by the relation

$$\vec{\mu} = g\mu_B \frac{\vec{J}}{\hbar} \quad (1)$$

where μ_B is the Bohr magneton $\mu_B = e\hbar/(2m_e) \approx 9.274 \times 10^{-24} \text{ J T}^{-1}$. Dirac theory of a free, point-like particle has $g = 2$ exactly. The experimentally observed deviation $a = (g - 2)/2$ from that value is called “anomaly” of the *g*-factor. For the “free” (unbound) electron, the anomaly is due to effects of quantum electrodynamics (QED) alone, whereas in highly charged ions, it is due to a number of effects related to the binding

situation, mainly due to relativistic effects, QED effects, and nuclear effects.^[3]

The magnetic moment of the unbound electron in units of the Bohr magneton has been measured to 2.7×10^{-13} relative accuracy by spectroscopy in a Penning trap.^[4,5] From this measurement, in combination with QED theory that relates the electron magnetic moment and the fine structure constant α ,^[6] the value of α has been determined to about four parts in 10^9 .^[4,5] This value agrees with a similarly precise value obtained from a complementary measurement,^[7] and the agreement is commonly seen as the current most stringent test of QED in the absence of external fields.

The magnetic moment of the electron when bound in a highly charged ion has been measured for several ion species up to lithium-like calcium (Ca^{17+}) by the application of the continuous Stern–Gerlach effect^[8] in Penning traps with a magnetic bottle.^[9] These measurements have yielded values of the electron magnetic moment with relative accuracies on the scale of 10^{-9} to 10^{-11} .^[10–14] From similar measurements with $^{12}\text{C}^{5+}$, the current best value of the atomic mass of the electron has been obtained.^[15,16] Also in the case of bound electrons, magnetic moment measurements are seen as valuable for an independent determination of the fine structure constant α .^[17]

Highly charged ions make an interesting object of study to this end, since the binding situation changes the value of the electron magnetic moment by up to about 20%, which is many orders of magnitude larger than the typical experimental uncertainty. The magnitude of this change roughly scales with the square of the nuclear charge state *Z* of the ion,^[3,18] hence making measurements at high values of *Z* potentially interesting.

Dr. M. Vogel, Dr. M. S. Ebrahimi, Z. Guo, A. Khodaparast, Dr. W. Quint
GSI Helmholtzzentrum für Schwerionenforschung
64291 Darmstadt, Germany
E-mail: m.vogel@gsi.de

Prof. G. Birkel
Institut für Angewandte Physik
TU Darmstadt, 64289 Darmstadt, Germany

Dr. W. Quint
Physikalisches Institut
Ruprecht Karls-Universität Heidelberg
69120 Heidelberg, Germany

 The ORCID identification number(s) for the author(s) of this article can be found under <https://doi.org/10.1002/andp.201800211>

DOI: 10.1002/andp.201800211

Figure 1 shows a cartoon as the example of a high- Z hydrogen-like ion like Bi^{82+} and the involved quantities: a single electron is bound to an atomic nucleus ($Z = 83$). The precession of the electron spin around the external magnetic field B_0 of the Penning trap at the Larmor frequency ω_L yields the desired magnetic moment μ and hence the electronic g -factor g_J by

$$\hbar\omega_L = \mu B_0 = g_J \mu_B B_0 \quad (2)$$

With the presently discussed experiment, the value of the nuclear g -factor g_I can be determined simultaneously with g_J , as will be detailed below.

In particular, for few-electron ions such as hydrogen-like ions and lithium-like ions, detailed theoretical predictions of magnetic moments exist,^[17,19–28] such that a systematic comparison of experiment and theory across a range of ion species allows to test calculations and their assumptions or in turn to extract properties of the electron and the nucleus.^[29,30] This particularly includes ion species heavier than those measured so far, which motivates measurements in a regime where the effects on the bound electrons are strongest.^[29]

In highly charged ions, such electron magnetic moment measurements are possible in two complementary ways, either by the continuous Stern–Gerlach effect applied to ions with zero-spin nuclei, in full similarity to the measurements,^[10–16] or by making use of the fact that in highly charged ions above a certain value of Z , the hyperfine structure of a few-electron ion becomes accessible for laser spectroscopy.^[3] Here, we discuss this latter approach by the ARTEMIS experiment^[31,32] with highly charged ions in a cryogenic Penning trap that is optimized for optical spectroscopy under large solid angles.^[33,34] This experiment is located at the HITRAP facility^[35] at GSI, Germany. We present the concept and current status of the experiment and discuss the possibility of Doppler-free optical spectroscopy of heavy highly charged ions cooled to a crystalline state by use of resistive cooling alone.

2. Experimental Section

The main goal of the measurement is a determination of the magnetic moment of the bound electron. **Figure 2** shows the magnetic moment (expressed by the g -factor, see Equation (1)) of the electron bound in hydrogen-like and lithium-like ions as a function of nuclear charge number Z . The solid lines represent the theory values. The indicated ions with nuclear charge states below $Z = 20$ have been measured so far, the others are prominent candidate ions. Note that on the scale of the figure, experiment and theory values are indistinguishable and experimental uncertainties disappear within the line thickness.

For ions with nonvanishing nuclear spin, the g -factor g_F of the whole ion is a combination of the g -factors of the bound electron and the nucleus. The expression

$$g_F = g_J \frac{F(F+1) + J(J+1) - I(I+1)}{2F(F+1)} - g_I \frac{F(F+1) + I(I+1) - J(J+1)}{2F(F+1)} \frac{m_e}{m_p} \quad (3)$$



Manuel Vogel is a researcher in the atomic physics department of the GSI Helmholtzzentrum für Schwerionenforschung in Darmstadt and is involved with the department's Penning trap experiments including ARTEMIS. His research interests are experiments and techniques employing Penning traps particularly in connection with precision spectroscopy of highly charged ions and studies of the interactions between highly charged ions and high-intensity lasers.



Gerhard Birkel is professor and head of the “Atoms-Photons-Quanta” group as well as Executive Director of the Institut für Angewandte Physik at Technische Universität Darmstadt. Together with Wolfgang Quint, he is Co-PI of the ARTEMIS collaboration. His research interests include laser cooling and high-resolution spectroscopy of highly charged ions in ion traps and storage rings, the

investigation of the properties of quantum-degenerate gases (e.g., Bose–Einstein condensates), quantum simulations, quantum computations, and quantum metrology with individual ultracold atoms and quantum-degenerate gases, the application of micro-optical systems to atom optics and ATOMTRONICS, and the advancement of the relevant laser systems.



Wolfgang Quint is a researcher at GSI Helmholtzzentrum für Schwerionenforschung in Darmstadt and a lecturer at Ruprecht-Karls-Universität Heidelberg. He received his Ph.D. at the University of Munich and has been a postdoc at Harvard University and at CERN. He works on precision experiments in ion traps for testing the theory of quantum electrodynamics and matter-antimatter symmetry, and for the determination of fundamental constants.

relates g_F to the g -factor of the bound electron g_J and the nuclear g -factor $g_I = \mu/(\mu_N I)$, where μ_N is the nuclear magneton and m_e and m_p are the electron and proton mass, respectively. The g -factors of the electron and the nucleus can both be determined when the magnetic moment of the ion is measured in two

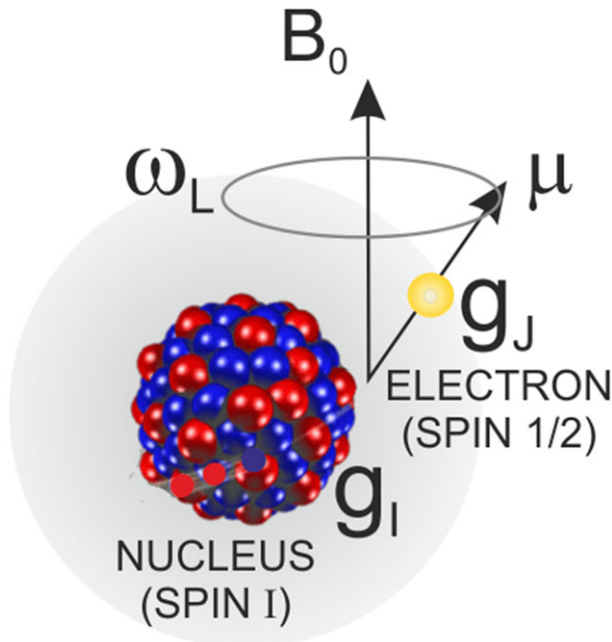


Figure 1. Cartoon of a hydrogen-like ion and the quantities involved: a single electron is bound to an atomic nucleus. The precession of the electron spin around the external magnetic field B_0 of the Penning trap at the Larmor frequency ω_L yields the magnetic moment μ and hence the electronic g -factor g_J .

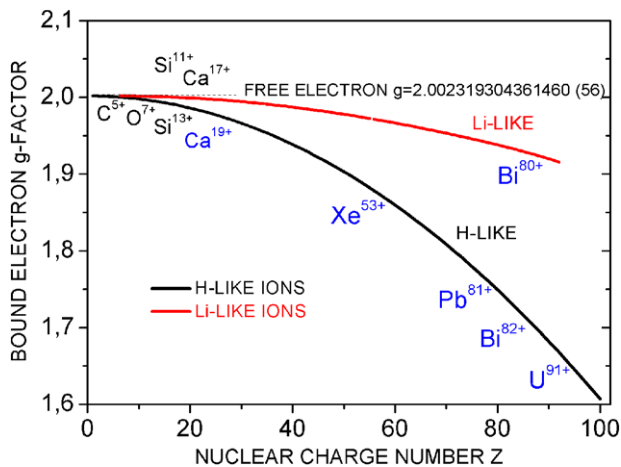


Figure 2. Theory predictions of the magnetic moment (g -factor) of the electron bound in hydrogen-like and lithium-like ions as a function of nuclear-charge number Z . The indicated ions with charge states below $Z = 20$ have been measured so far; the others are prominent candidate ions. Note that on this scale, experiment and theory values are indistinguishable and experimental uncertainties vanish within the line thickness.

different hyperfine states F and F' , that is, when the two g -factors g_F and $g_{F'}$ are measured for states with different F in one ion, namely for $F = I - 1/2$ and $F' = F + 1 = I + 1/2$. Then, the g -factors of the bound electron and the nucleus (g_J and g_I) can be written in terms of the experimentally obtained values by^[31]

$$g_J = (I + 1)g_{F'} - Ig_F - \delta_Q Q \left(\frac{m_e c}{\hbar} \right)^2 \frac{2(I + 1)}{2I - 1} \quad (4)$$

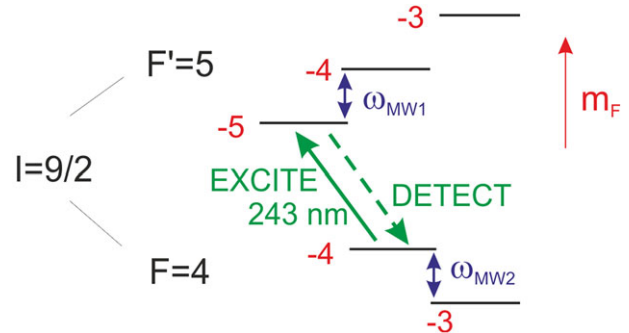


Figure 3. Relevant part of the level scheme of $^{209}\text{Bi}^{82+}$ (nuclear spin $I = 9/2$ leading to hyperfine levels $F = 4$ and $F' = 5$) for double-resonance spectroscopy: resonant irradiation at either ω_{MW1} or ω_{MW2} reduces the population in the closed optical cycle at 243 nm and thus allows a determination of both these microwave frequencies.

and

$$g_I = -\frac{m_p}{m_e} \frac{g_{F'} + g_F + \delta_Q Q \left(\frac{m_e c}{\hbar} \right)^2}{2(1 - \delta_\mu)} \frac{3}{I(2I - 1)} \quad (5)$$

Here, Q is the electric quadrupole moment of the nucleus, and δ_μ and δ_Q are small corrections that can be obtained from theory to high accuracy.^[31] The application of this method to various families of ion level schemes has been discussed in ref. [31].

As an example, **Figure 3** shows the relevant part of the hyperfine structure of a $^{209}\text{Bi}^{82+}$ ion. The nucleus has spin $I = 9/2$, hence the hyperfine levels are $F = 4$ and $F' = 5$. These are separated by a magnetic dipole transition in the near-ultraviolet regime at a wavelength of 243 nm. The external magnetic field B_0 of the Penning trap leads to a Zeeman splitting of each of the hyperfine levels into $2F + 1$ sublevels. At the present magnetic field strength of 7 T, these sublevels are separated by microwave frequencies of several tens of gigahertz. In this example, the measurement of ω_{MW1} (for $F = 4$) yields the ionic g_F , while the measurement of ω_{MW2} (for $F' = 5$) yields the ionic $g_{F'}$.

Due to the factor m_e/m_p in Equation (3) the potential relative accuracy of g_I is about three orders of magnitude smaller than the ones of g_J and g_F . However, assuming a relative accuracy of the microwave frequency measurement on the level of parts per billion (ppb), a determination of the nuclear magnetic moment is possible on the level of parts per million (ppm) and hence comparable to most other measurements. Note that for a few-electron ion, the diamagnetic shielding of the nucleus is well calculable. This is an advantage with respect to nuclear magnetic resonance (NMR) measurements and allows a benchmarking of shielding models.

In general, the application of this spectroscopy scheme requires the hyperfine transition to be addressable by laser light. For the hyperfine structure of the $(1s) \ ^2S_{1/2}$ ground state of hydrogen-like ions, the transition energy is given by^[3]

$$E_{HFS} = \frac{4}{3} \alpha(Z\alpha)^3 g_I \frac{m_e}{m_p} \frac{2I + 1}{2} m_e c^2 A_{1s} (1 - \delta_{1s}) \quad (6)$$

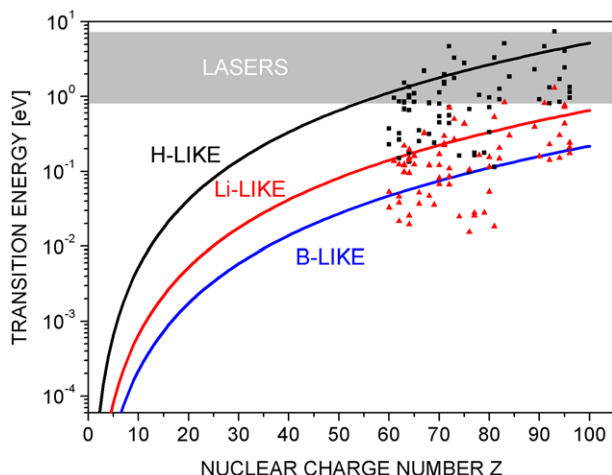


Figure 4. Hyperfine transition energies as a function of nuclear-charge number for hydrogen-like, lithium-like, and boron-like ions. Lines: scaling laws assuming $I = 5/2$ and $g_I = 1$. Dots: detailed calculations for hydrogen-like and lithium-like ions with $Z > 60$.

where

$$A_{1s} = \frac{1}{\kappa(2\kappa - 1)} \quad \text{and} \quad \kappa = \sqrt{1 - (Z\alpha)^2} \quad (7)$$

This energy value represents the “classical” ground-state hyperfine splitting energy that is multiplied by the factor A_{1s} to correct for the relativistic energy of the $1s$ electron. Here, κ is related to the angular momentum of the electron, and the factor $(1 - \delta_{1s})$ accounts for the finite size of the nucleus including corresponding QED contributions.^[3] Likewise, for lithium-like ions, the hyperfine transition energy of the $(1s^2 2s)^2 S_{1/2}$ ground state is given by^[3]

$$E_{HFS} = \frac{1}{6} \alpha (Z\alpha)^3 g_I \frac{m_e}{m_p} \frac{2I + 1}{2} m_e c^2 A_{2s} (1 - \delta_{2s}) \quad (8)$$

with the relativistic correction factor

$$A_{2s} = 2 \frac{2(1 + \kappa) + \sqrt{2(1 + \kappa)}}{(1 + \kappa)^2 \kappa (4\kappa^2 - 1)} \quad (9)$$

and the factor $(1 - \delta_{2s})$ that accounts for the finite size of the nucleus including corresponding QED contributions and electron-electron interaction.^[3]

Figure 4 shows the hyperfine transition energy as a function of the nuclear charge number Z for hydrogen-like, lithium-like, and boron-like ions. To indicate the overall trend, the solid lines assume a nuclear spin of $I = 5/2$ and a nuclear magnetic moment of $1 \mu_N$. The data points show the values when the correct values of I and g_I are used. We have restricted this plot to the region with $Z > 60$, since below, the transitions are far outside the optical (and near-optical) regime that is indicated by the grey area.

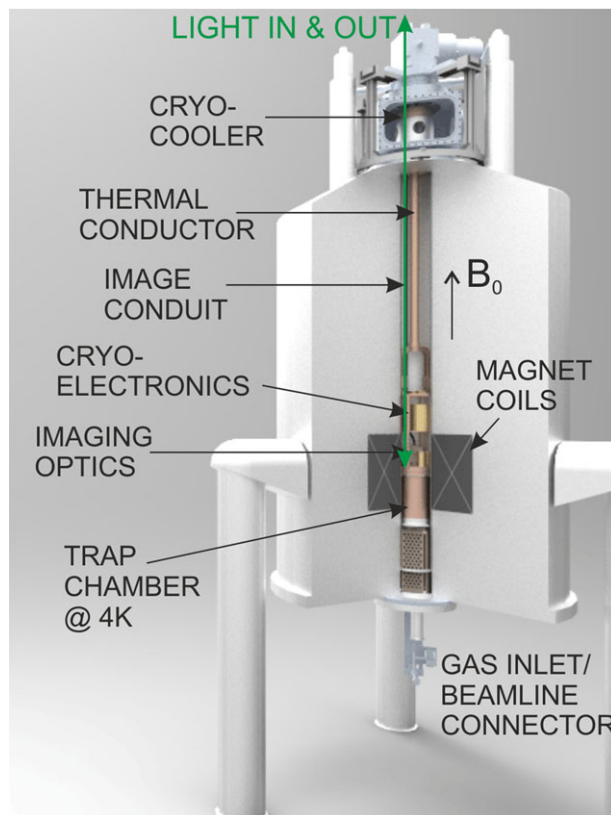


Figure 5. Cutout of the setup consisting of a cryogenic Penning trap arrangement in the center of a superconducting magnet. The light (excitation laser and fluorescence signal) is guided to and from the trap via an image conduit.

The linewidth of a ground-state magnetic dipole transition from the excited to the lower hyperfine state in a hydrogen-like ion is given by^[3]

$$\Gamma_{HFS} = \frac{4\alpha\omega^3 \hbar^2 I (2k + 1)^2}{27m_e^2 c^4 (2I + 1)} \quad (10)$$

where ω is the transition frequency. The linewidth of ions in the laser-accessible region reaches up to several kilohertz. The corresponding small photon scattering rate is a challenge for spectroscopy; however, the relative accuracies are potentially high when cold ions are used. To this end, we employ resistive cooling to temperatures of a few Kelvin, as will be detailed below.

3. Experimental Setup

3.1. Overview

The setup (see **Figure 5**) consists of two adjacent cylindrical Penning traps located at the center of a superconducting magnet. The traps and their detection electronics are cooled to liquid-helium temperature by a pulse-tube cryo-cooler. One trap is designed for charge breeding of highly charged ions from gas by an electron beam from a field emission tip. The electron energy can be

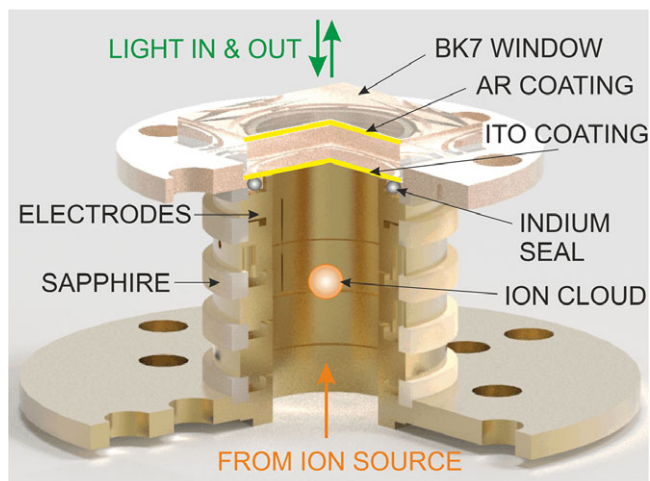


Figure 6. Cutout of the dedicated spectroscopy trap, which is a half-open cylindrical Penning trap with a window endcap that has a conductive coating on the inside. The excitation laser beam enters from above, ions from below. Fluorescence is collected through the window.

chosen up to several kiloelectronvolts such that the production of ions like Ar^{13+} for test purposes is routinely feasible. Currently, the trap system is being connected to the low-energy beamline^[36] of the HITRAP facility, from where bunches of highly charged ions including $^{207}\text{Pb}^{81+}$, $^{209}\text{Bi}^{82+}$, and $^{235}\text{U}^{91+}$ are foreseen to be delivered to upcoming experiments.^[35] The spectroscopy is performed in a dedicated Penning trap with an optical window, to and from which light is guided by an image conduit connecting the trap to the outside laser lab and image detection via a CCD camera.

3.2. Spectroscopy Trap

For the present optical spectroscopy, a large solid angle of detection is favorable, in particular, due to the comparatively low fluorescence rates of the magnetic dipole transitions under investigation. The confining potential, however, needs to be highly harmonic, which forbids electrode openings such as slits, holes, or meshes. To this end, the ARTEMIS experiment features a dedicated kind of trap, a so-called “half-open” cylindrical Penning trap with a conducting window endcap electrode (see **Figure 6**). The concept of a half-open cylindrical trap has initially been presented in detail in ref. [34] It is a variation of a closed cylindrical Penning trap, with one closed endcap replaced by open cylindrical electrodes to allow injection and ejection of particles, and the other endcap being electrically closed while optically transparent, which in the present case is realized by a window with a conductive coating of indium tin oxide (ITO).^[33] This special electrode arrangement has the confinement region in close proximity to the optically open endcap, and thus features a largely enhanced solid angle of detection as compared to the standard open-endcap design.^[33] Tests have shown that highly charged ions can be confined for periods of days in this trap under well-defined conditions.

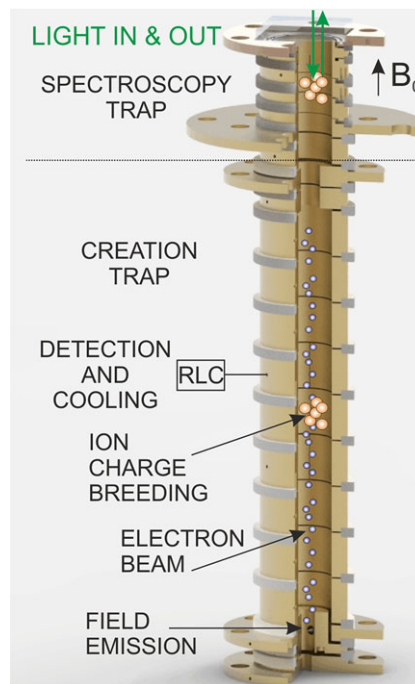


Figure 7. Cutout of the complete trap arrangement including the trap for the creation of highly charged ions by charge breeding in an electron beam from a field-emission point. Note that the spectroscopy trap above the dotted line is the one detailed in **Figure 6**. Upon creation, ions are transferred to the spectroscopy trap for the g -factor measurements.

4. Ion Preparation and Cooling

By use of the internal ion source, ensembles of highly charged argon ions have been produced from injected gas. As a source of small amounts of argon gas, a baffle-like structure at liquid-helium temperature is filled with argon gas that freezes out. When ions need to be produced, a current through an attached resistor is used to temporarily heat the baffles to temperatures around 35 K, hence releasing gas from the inner surfaces. This gas then enters the creation part of the trap setup where it is ionized by an electron beam from a field emission tip. **Figure 7** shows a cutout of the complete trap arrangement with the trap for the creation of highly charged ions by charge breeding in an electron beam from a field emission point below the spectroscopy trap.

In this so-called “creation trap,” ensembles of argon ions have been produced and cooled by resistive cooling of the axial motion.^[37] Typical spectra contain argon ions of charge states between 8^+ and 16^+ (see, e.g., the inset of **Figure 8**) as well as tungsten ions of higher charge states that originate from the field emission tip. From the observed space-charge shift of the axial oscillation frequency, ion number densities of the order of 10^6 per cm^3 can be derived. Detection and resistive cooling of the axial motions is performed by ramping of the trap voltage such that the axial oscillation frequency of all ion species subsequently becomes resonant with the RLC circuit which is cooled to liquid-helium temperature. The circuit is used for both cooling and detection and is resonant at a frequency of $\omega_R = 2\pi \times 741.23$ kHz

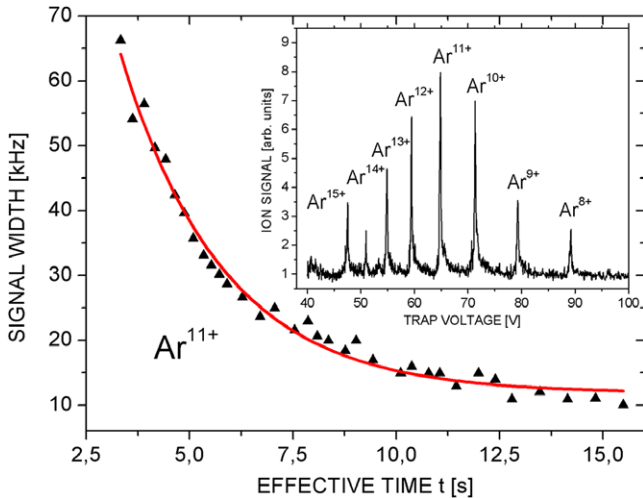


Figure 8. Spectral width of the detected signal of Ar^{11+} ions as a function of the effective cooling time. The curve is an exponential decay fitted to the data. Inset: spectrum of confined argon-ion charge states as produced by the internal ion source.

with a quality factor of $Q = 900$. Its inductance is about 3 mH, and hence in resonance it represents a resistance of

$$R = QL\omega_z \approx 12.5 \text{ M}\Omega \quad (11)$$

The corresponding cooling time constant of the ions is given by^[37]

$$\tau = \frac{mD^2}{Rq^2} \quad (12)$$

where m is the ion mass, q is the ion charge, and $D \approx 40$ mm is the effective distance of the electrodes used for cooling and detection. Under the present conditions, typical cooling time constants are of the order of a few seconds.

To illustrate the effect of resistive cooling, Figure 8 shows the spectral width of the detected signal of Ar^{11+} ions as a function of the cooling time (for details see ref. [37]), to which an exponential decay with a time constant of a few seconds can be fitted. This time constant is in agreement with theoretical expectations for the given conditions.^[37] From the width of the signal upon cooling, the temperature of the ion ensemble can be derived. This is true since under the present conditions, the thermalization of the ensemble via the Coulomb interaction is considerably faster than the resistive cooling.^[37] Also, the spectral width of the RLC circuit used for detection is negligible with respect to the width of the signal. This width is given by^[37]

$$\frac{\delta\omega_z}{\omega_z} \approx \frac{3C_4}{C_2^2} \frac{k_B T}{q U_0} + \frac{15C_6}{C_2^3} \left(\frac{k_B T}{q U_0} \right)^2 \quad (13)$$

From the present trap, potential parameters $C_2 = 0.5631$, $C_4 = 0.0010$, and $C_6 = 0.0502$ (calculated from the measured trap geometry according to the formalism in ref. [38]) and the measured asymptotic width of about 7 kHz, an ion temperature of about

7.5 K can be derived, which is slightly above the ambient temperature of liquid helium. At the presently estimated ion number densities of the order of 10^6 per cm^3 , this corresponds to a value of the plasma parameter Γ of around 2–5, for which a fluid-like behavior of the ion ensemble is expected. The plasma parameter measures the ion–ion correlation energy in relation to the ion kinetic energy and is given by^[39,40]

$$\Gamma = \frac{q^2}{4\pi\epsilon_0 a k_B T} \quad (14)$$

where the volume $a^3 = 3/(4\pi n)$ follows from the ion number density n . For values $\Gamma \ll 1$, an ion ensemble behaves gas-like with negligible motional ion–ion correlation, that is, largely independent ion motion. Around $\Gamma \approx 2$, this behavior transitions into fluid-like correlation between the ions, and for $\Gamma > 170$, crystalline structures have been observed in Penning traps.^[1,39,40]

At present, indications of a transition of the ion ensemble from a state with low correlation to a significantly correlated axial motion have been observed as a discontinuous spectral behavior during cooling around these values of the plasma parameter.^[37] Note the factor q^2 in the numerator of the plasma parameter. From this, candidate ions for the envisaged optical spectroscopy measurements^[31] such as Bi^{82+} or U^{91+} are expected to form ion crystals by mere resistive cooling. At the envisaged experimental parameters, the axial ion oscillation amplitude becomes comparable or smaller than the wavelength of the transition of interest, in which case a first-order Doppler effect is absent, facilitating precision optical spectroscopy.

5. Summary

We have presented a concept and experimental setup for spectroscopic precision measurements of the magnetic moment (g -factor) of the electron bound in a highly charged ion. This opens the possibility for stringent tests of calculations in the framework of theory of highly charged ions and in turn gives access to fundamental constants such as the fine structure constant and the atomic mass of the electron. Such measurements are possible when the electron is bound in a highly charged ion confined in a Penning trap. Two complementary approaches using Penning trap techniques are possible, one via the continuous Stern–Gerlach effect applied to ions with vanishing nuclear spin, the other via double-resonance spectroscopy applied to ions with nonvanishing nuclear spin. The prior approach has been realized in the Mainz/Heidelberg g -factor experiments,^[29] the latter approach is about to be realized in the present ARTEMIS experiment in the framework of the HITRAP project. We have presented the concept, setup, and status of this latter experiment, currently under commissioning with internally produced highly charged ions. We have presented measurements of resistive ion cooling, leading to a fluid-like state of ensembles of ions such as Ar^{13+} . From common ion plasma theory, it is expected that ions of much higher charge states form ion crystals which facilitate Doppler-free precision spectroscopy. A connection to the low-energy beamline of HITRAP facility is under construction,

from where ions such as Pb^{81+} , Bi^{82+} , or U^{91+} are to be delivered to experiments including ARTEMIS.

Acknowledgements

This article is part of the Special Issue on *The Revised SI: Fundamental Constants, Basic Physics and Units*, highlighting the revision and redefinition of the International System of Units (SI) to come into effect in May 2019.

Conflict of Interest

The authors declare no conflict of interest.

Keywords

electron magnetic moment, highly charged ions, Penning traps

Received: June 22, 2018

Revised: August 21, 2018

Published online: October 8, 2018

- [1] M. Vogel, *Particle Confinement in Penning Traps*, Springer, Heidelberg, Germany **2018**.
- [2] M. Vogel, W. Quint, *Ann. Phys.* **2013**, 525, 505.
- [3] T. Beier, *Phys. Rep.* **2000**, 339, 79.
- [4] D. Hanneke, S. Fogwell, G. Gabrielse, *Phys. Rev. Lett.* **2008**, 100, 120801.
- [5] D. Hanneke, S. F. Hoogerheide, G. Gabrielse, *Phys. Rev. A* **2011**, 83, 052122.
- [6] T. Aoyama, M. Hayakawa, T. Kinoshita, M. Nio, *Phys. Rev. D* **2015**, 91, 033006.
- [7] R. Bouchendira, P. Cladé, S. Guellati-Khélifa, F. Nez, F. Biraben, *Phys. Rev. Lett.* **2011**, 106, 080801.
- [8] R. S. Van Dyck, Jr., P. B. Schwinberg, H. G. Dehmelt, *Phys. Rev. D* **1986**, 34, 722.
- [9] M. Vogel, G. Birkel, D. von Lindenfels, W. Quint, M. Wiesel, *Appl. Phys. B* **2013**, 114, 63.
- [10] H. Häffner, T. Beier, N. Hermanspahn, H.-J. Kluge, W. Quint, S. Stahl, J. Verdú, G. Werth, *Phys. Rev. Lett.* **2000**, 85, 5308.
- [11] J. Verdú, S. Djekic, S. Stahl, T. Valenzuela, M. Vogel, G. Werth, T. Beier, H.-J. Kluge, W. Quint, *Phys. Rev. Lett.* **2004**, 92, 093002.
- [12] S. Sturm, A. Wagner, B. Schabinger, J. Zatorski, Z. Harman, W. Quint, G. Werth, C. H. Keitel, K. Blaum, *Phys. Rev. Lett.* **2011**, 107, 023002.
- [13] A. Wagner, S. Sturm, F. Köhler, D. A. Glazov, A. V. Volotka, G. Plunien, W. Quint, G. Werth, V. M. Shabaev, K. Blaum, *Phys. Rev. Lett.* **2013**, 110, 033003.
- [14] F. Köhler, K. Blaum, M. Block, S. Chenmarev, S. Eliseev, D. A. Glazov, M. Goncharov, J. Hou, A. Kracke, D. A. Nesterenko, Y. N. Novikov, W. Quint, E. M. Ramirez, V. M. Shabaev, S. Sturm, A. V. Volotka, G. Werth, *Nat. Comm.* **2016**, 7, 10246.
- [15] S. Sturm, F. Köhler, J. Zatorski, A. Wagner, Z. Harman, G. Werth, W. Quint, C. H. Keitel, K. Blaum, *Nature* **2014**, 506, 467.
- [16] F. Köhler, S. Sturm, A. Kracke, G. Werth, W. Quint, K. Blaum, *J. Phys. B* **2015**, 48, 144032.
- [17] V. M. Shabaev, D. A. Glazov, N. S. Oreshkina, A. V. Volotka, G. Plunien, H.-J. Kluge, W. Quint, *Phys. Rev. Lett.* **2006**, 96, 253002.
- [18] A. V. Volotka, D. A. Glazov, G. Plunien, V. M. Shabaev, *Ann. Phys.* **2013**, 525, 636.
- [19] V. M. Shabaev, V. A. Yerokhin, *Phys. Rev. Lett.* **2002**, 88, 091801.
- [20] D. A. Glazov, V. M. Shabaev, I. I. Tupitsyn, A. V. Volotka, V. A. Yerokhin, G. Plunien, G. Soff, *Phys. Rev. A* **2004**, 70, 062104.
- [21] D. A. Glazov, A. V. Volotka, V. M. Shabaev, I. I. Tupitsyn, G. Plunien, *Phys. Rev. A* **2010**, 81, 062112.
- [22] V. A. Yerokhin, K. Pachucki, Z. Harman, C. H. Keitel, *Phys. Rev. Lett.* **2011**, 107, 043004.
- [23] J. Zatorski, N. S. Oreshkina, C. H. Keitel, Z. Harman, *Phys. Rev. Lett.* **2012**, 108, 063005.
- [24] K. Pachucki, A. Czarnecki, U. D. Jentschura, V. A. Yerokhin, *Phys. Rev. A* **2005**, 72, 022108.
- [25] A. Czarnecki, R. Szafron, *Phys. Rev. A* **2016**, 94, 060501(R).
- [26] V. A. Yerokhin, Z. Harman, *Phys. Rev. A* **2017**, 95, 060501(R).
- [27] V. M. Shabaev, D. A. Glazov, A. V. Malyshev, I. I. Tupitsyn, *Phys. Rev. Lett.* **2017**, 119, 263001.
- [28] V. A. Yerokhin, K. Pachucki, M. Puchalski, Z. Harman, C. H. Keitel, *Phys. Rev. A* **2017**, 95, 062511.
- [29] S. Sturm, M. Vogel, F. Köhler-Langes, W. Quint, K. Blaum, G. Werth, *Atoms* **2017**, 5, 4.
- [30] S. Sturm, A. Wagner, M. Kretschmar, W. Quint, G. Werth, K. Blaum, *Phys. Rev. A* **2013**, 87, 030501(R).
- [31] W. Quint, D. Moskovkin, V. M. Shabaev, M. Vogel, *Phys. Rev. A* **2008**, 78, 032517.
- [32] D. von Lindenfels, M. Wiesel, D. A. Glazov, A. V. Volotka, M. M. Sokolov, V. M. Shabaev, G. Plunien, W. Quint, G. Birkel, A. Martin, M. Vogel, *Phys. Rev. A* **2013**, 87, 023412.
- [33] M. Wiesel, G. Birkel, M. S. Ebrahimi, A. Martin, W. Quint, N. Stallkamp, M. Vogel, *Rev. Sci. Instrum.* **2017**, 88, 123101.
- [34] D. von Lindenfels, M. Vogel, G. Birkel, W. Quint, M. Wiesel, *Hyp. Int.* **2014**, 227, 197.
- [35] H.-J. Kluge, T. Beier, K. Blaum, L. Dahl, S. Eliseev, F. Herfurth, B. Hoffmann, O. Kester, S. Koszudowski, G. Maero, W. Nörthershäuser, J. Pfister, W. Quint, U. Ratzinger, A. Schempp, R. Schuch, T. Stöhlker, R. C. Thompson, M. Vogel, G. Vorobjev, D. F. A. Winters, G. Werth, *Adv. Quantum Chem.* **2007**, 53, 83.
- [36] Z. Andelkovic, G. Birkel, S. Fedotova, V. Hannen, F. Herfurth, K. König, N. Kotovskiy, B. Maaß, J. Vollbrecht, T. Murböck, D. Neidherr, W. Nörthershäuser, S. Schmidt, M. Vogel, G. Vorobjev, C. Weinheimer, *Nucl. Inst. Meth A* **2015**, 795, 109.
- [37] M. S. Ebrahimi, Z. Guo, M. Wiesel, G. Birkel, W. Quint, M. Vogel, *Phys. Rev. A* **2018**, 98, 023423.
- [38] G. Gabrielse, L. Haarsma, S. L. Rolston, *Int. J. Mass Spectr. Ion Proc.* **1989**, 88, 319.
- [39] L. R. Brewer, J. D. Prestage, J. J. Bollinger, W. M. Itano, D. J. Larson, D. J. Wineland, *Phys. Rev. A* **1988**, 38, 859.
- [40] R. C. Thompson, *Contemp. Phys.* **2015**, 56, 63.